

Classification of Shoeprint Images Using Directional Filterbanks

Lahouari Ghouti, Ahmed Bouridane and Danny Crookes

School of Computer Science, Queen's University of Belfast,
Belfast BT7 1NN, United Kingdom.

Email: {L.Ghouti, A.Bouridane, D.Crookes}@qub.ac.uk

Keywords: Scene of crime evidence, shoeprint images, directional filterbanks, directional energy, image retrieval.

During a forensic investigation, a shoeprint impression lifted from SoC is compared against shoeprint databases. Several databases of shoeprints can be available, including [1, 7]:

Abstract

With the abundance of evidence data collected from scenes of crime (SoC), shoeprint (or soleprint) traces usually constitute one of the hardest types of evidence for a criminal to remove before leaving the SoC. Traditional approaches to shoeprint representations attempt to classify shoeprint images based on a number of possible patterns. Such approaches are difficult to implement in an automatic fashion without the intervention of a forensic specialist. In this paper, we propose a fully-automated system to assist forensic specialists in rapidly classifying a shoeprint image found in a scene of crime (SoC). The proposed multiresolution-based system uses directional filterbanks (DFBs) to capture both local and global details in a shoeprint in a compact representation called *ShoeHash*. Experimental results based on forensic shoeprint databases of more than 1000 images are presented to validate the effectiveness of the proposed system in extracting shoeprint features and achieving good performance.

Keywords: forensics, directional filterbank (DFB), contourlets, shoeprint classification, feature extraction.

1 Introduction

Recent developments in forensic science have resulted in large numbers of SoC images being collected for recording and analysis. Shoeprint images are no exception. Sole marks from a scene of crime (SoC) are acquired through photography, gel, or electrostatic lifting or by performing a cast on a soil impression. Therefore, acquired images can be: 1) three-dimensional¹ as in the case of an impression in a clay, sand, and snow. In this case, these marks are recovered from a SoC by casting them with dental stone and photographs are taken before making the cast. 2) two-dimensional, usually found on surfaces such as carpet, stone, and wood. Most of the time, these marks are not visible under standard conditions. To make these marks visible, several procedures are adopted [1]. Then, the acquired images are scanned and stored in a digital format in a shoeprint database such as REBEZO [1] or SoleMate [2].

¹In this paper, the proposed system does not consider three-dimensional shoeprint images.

1. A database containing standard shoeprint marks representing most of the available shoes on the market.
2. A database containing shoeprint impressions lifted from other SoCs (for relating different crime scenes).
3. A database containing shoeprint profiles of shoes from suspects.

Currently most of the available forensic procedures consist of a laborious manual analysis, involving a manual search against paper catalogues or a computer-based database. Due to the time-consuming nature of current forensic practices, the inclusion of shoeprint evidence in crime investigation has been severely hampered. For instance, Geradts and Keijzer [1] report that, in 1993, of 14000 shoeprint marks collected from SoCs, only 2000 marks were compared against suspects' shoeprints. From these, only 500 identifications were possible. Bodziak [3] indicates that shoeprint evidence from crime scenes is more frequently present than fingerprints. In Daubert rulings [4], the US Court upholds, as a general principle, the relevance and reliability of the "science" of footwear impression evidence in criminal cases generally. Girod [5] suggests that 30% of the burglary scenes provide valid evidence and usable shoeprints. Also, 35% of SoCs present shoeprint traces that can be used as scientific evidence in forensic science as reported in a study conducted in several jurisdictions in Switzerland. However, to increase the reliability of decision making in such forensic settings and assist the forensic specialist in his/her duties, there must be an effective and precise framework for searching, browsing, querying, and interacting with these important collections and such processes are expected to be carried out in a timely manner. In response to these concerns, systems, known as QBIC (Query By Image Content), have been recognized as a potential solution for this fast-growing "digital forensic world". Geradts et al. [1] propose a *semi-automated* system based on a shoeprint database called REBEZO. Shoeprint images are first segmented into distinguishable shapes and patterns. For each shape, Fourier features and moment invariants are calculated. Then, Fourier features are classified using a feed-forward neural network that consists of a single hidden layer. In this paper, we propose a new multiresolution-based shoeprint image matching and classification method that is robust to diverse affine and geometric alterations of

the input shoeprint. Thanks to the directional discrimination of the multiresolution representation, the proposed method takes into consideration the directional information content of the shoeprint images. Furthermore, the directional energies are captured in a compact representation that constitutes a robust feature vector for matching and classification purposes. Several (32 or 16) energy-dominant image blocks are extracted to form the directional feature vector. Shoeprint features are then extracted from the the selected blocks using multiresolution-based directional filter banks (DFBs). DFBs are known to effectively represent the intrinsic geometrical structure of the input image [6, 8]. Using the resulting directional subbands, we estimate the directional energy content of each selected block. To accommodate the variations in the spatial intensity across the shoeprint image, we propose to use the normalized energy content instead of the energy content itself. Furthermore, for the compactness of the shoeprint representation requirement, *ShoeHash*, it is necessary to set a threshold to discriminate between the most dominant sub-blocks from the least-dominant ones in terms of the directional energies. The least-dominant sub-blocks, considered as noise, are set to zero. Finally, based on a variance-weighted similarity distance, the matching between the input image and the database content is performed to retrieve the most similar shoeprint image. The rest of the paper is organized as follows. In Section II, we provide a brief overview of the directional filter banks (DFBs) on which shoeprint matching algorithm is based. Details attendant to the feature extraction and matching process are described in Section III. Section IV presents experimental results. Finally, conclusions are drawn in Section V.

2 Construction of Directional Features

Shoeprint images vary in size, contrast, and are located randomly in lifted images. Furthermore, image background can be contaminated by random noise such as blur, lines, or scratches. In the proposed algorithm, noise reduction and/or removal can be achieved by thresholding the high frequency coefficients. Unlike regular multiresolution analysis (MRA), DFBs define a multiresolution representation where directional features are efficiently captured. In this paper, we apply DFBs to construct a directional image. Let $I(x; y)$ denote the gray-level pixel at location $(x; y)$ of an $N \times N$ image. The spatial-domain image, I , is transformed to the multiresolution domain by the 2D DFB transformation as illustrated in Figure 1.

2.1 Directional Filterbanks

In [6], Bamberger and Smith pioneered the concept of a maximally decimated 2-D DFB representation while achieving perfect reconstruction. Their formulation can be efficiently

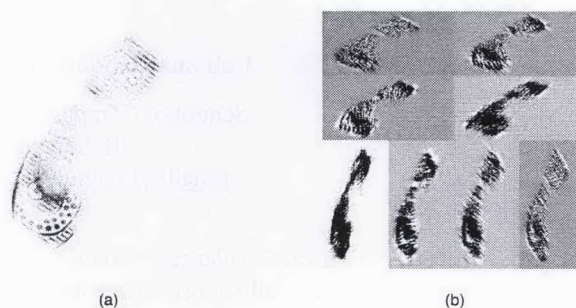


Figure 1: (a) A 512×512 shoe print image. (b) DFB subbands of size 256×128 lower blocks and size 128×256 upper blocks.

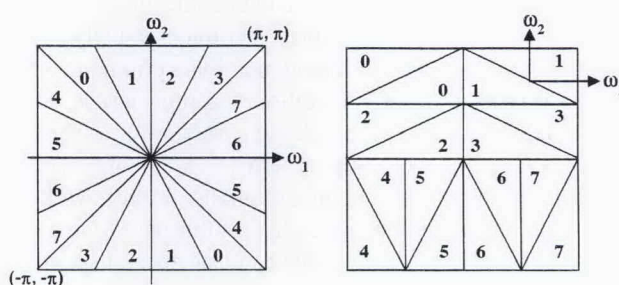


Figure 2: Frequency partitioning of the input where $l = 3$ (left). Eight decomposition subbands (right).

implemented via a l -level tree-structured decomposition that leads to 2^l subbands with wedge-shaped frequency partition as shown in Figure 2.

The original formulation of Bamberger and Smith [6] involves input modulation and diamond-shaped filters as illustrated in Figure 3. Bamberger's solution [6] produces visually distorted subband images, as the modulation and resampling operations introduce the undesirable effect of "frequency scrambling".

The DFB structure, as shown in Figure 3, basically consists of lowpass (H_0) and highpass (H_1) filters, quincunx downsamplers (Q), diamond conversion matrices (R), modulators ($e^{-j\omega_1\pi}$), and postsampling matrices (B). The spectrum of the image image, $I(x, y)$, is varied by the modulator to allow a directional repartition of the image spectrum. The quincunx downsampler reduces the sampling rate of the image and rotates it by 45 degrees. Do and Vetterli [8] propose an formulation of DFB based on quincunx filter bank (QFB) with only fan filters. Do's solution avoids the modulation of the input image and has a simplified rule for expanding the decomposition tree. The wedge-shaped frequency partition of the DFB is realized by an appropriate combination of directional frequency splitting by the fan QFB's and the rotation operations done by resampling.

Do and Vetterli [8] propose the structure, shown in Figure

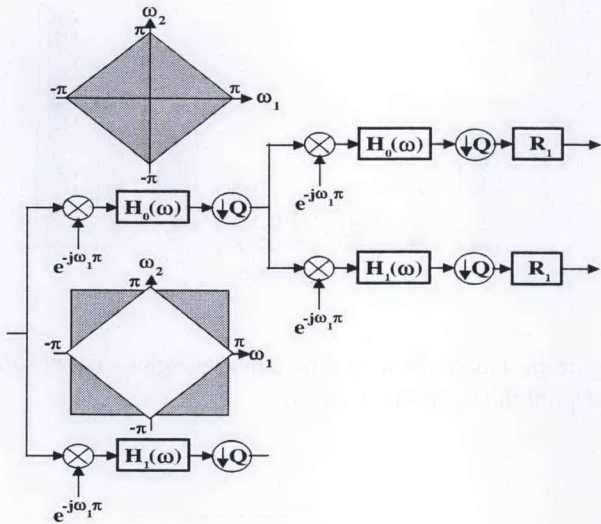


Figure 3: First two levels of eight-band Bamberger DFB decomposition.

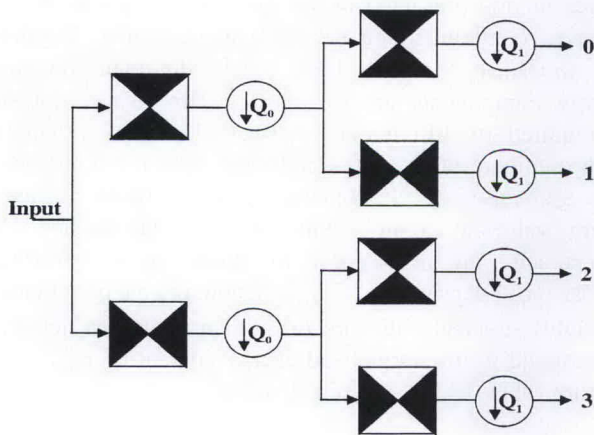


Figure 4: First two levels of Do's [8] solution.

4, to obtain a four directional frequency partitioning for the first two decomposition levels. In these levels, the sampling matrices can be either Q_0 or Q_1 such that the overall sampling after the first two levels is $Q_0Q_1 = 2 \cdot I_2$, where I_2 is a 2×2 identity matrix or the overall downsampling is 2 in each image dimension. Furthermore, based on the multirate identity, the second-level filters can be interchanged with the sampling matrix Q_0 . Based on this interchange, the fan filter is transformed into an equivalent filter with a quadrant frequency response. The quincunx sampling matrix Q can be either Q_0 or Q_1 defined below:

$$Q_0 = \begin{pmatrix} 1 & -1 \\ 1 & 1 \end{pmatrix}, \quad Q_1 = \begin{pmatrix} 1 & 1 \\ -1 & 1 \end{pmatrix} \quad (1)$$

Q_0 and Q_1 are possible representations of the two-dimensional quincunx sub-lattice [8]. The resampling operators, $R_k, k = 1, 2, 3, 4$ are based on one of the four basic *unimodular* matrices defined below:

$$R_1 = \begin{pmatrix} 1 & 1 \\ 0 & 1 \end{pmatrix}, \quad R_2 = \begin{pmatrix} 1 & -1 \\ 0 & 1 \end{pmatrix}, \quad (2)$$

$$R_3 = \begin{pmatrix} 1 & 0 \\ 1 & 1 \end{pmatrix}, \quad R_4 = \begin{pmatrix} 1 & 0 \\ -1 & 1 \end{pmatrix},$$

In this paper, we propose the use of the DFB structure, defined in [8], where the design of the filters is achieved through a ladder structure where all the filtering operations are separable. The analysis stage is based on a third-order decomposition of $N \times N$ images leading to eight subbands where the first half of the subbands has a size of $N/4 \times N/2$, while the other half has a size of $N/2 \times N/4$, respectively.

3 DFB-Based Processing and Feature Extraction

For feature extraction, each of the selected energy-dominant blocks is decomposed into $2^l, l = 3$ directional subbands using the ladder-based DFB. Then, using the resulting subbands, the directional energy of each block is estimated. In most situation, shoeprint images consist of patterns [7]. These patterns are characterized by strong directionality and, therefore, this directional information can be exploited as shoeprint features. In order to extract these features, a DFB representation can be effectively used. In this paper, for feature extraction, energy-dominant blocks are selected from the original shoeprint. Then, these blocks are decomposed into eight directional subband outputs using the DFB, and the directional energy of each block can be obtained from the resulting subbands. Let $f_{BLK}^\theta(x, y)$ denote the coefficient at position (x, y) of

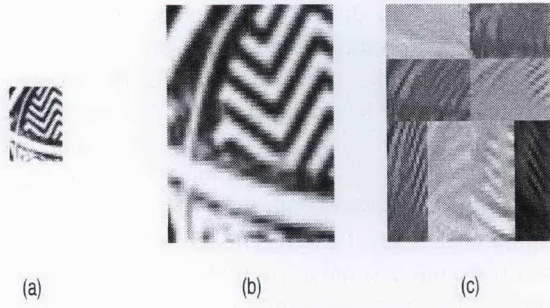


Figure 5: (a) Selected block in a shoeprint image. (b) Zoomed block. (c) DFB subbands of selected block.

the subband θ corresponding to an image block. The energy E_{BLK}^θ of a selected block associated with subband θ is defined as:

$$E_{BLK}^\theta = \sum_{x,y \in BLK} |f_{BLK}^\theta(x,y)|, \quad \theta = 0, 1, 2, \dots, 7 \quad (3)$$

Using $M \times M$ images, the DFB subbands corresponding to the orientations $\theta = 0, 1, 2, 3$ have a size of $M/4 \times M/2$, while those corresponding to the orientations $\theta = 4, 5, 6, 7$ have a size of $M/2 \times M/4$, as illustrated in Figure 1 and explained in Section 2.1. Similarly, for $m \times m$ image blocks, the first half of the resulting subbands has a size of $m/4 \times m/2$, while the other half has a size of $m/2 \times m/4$, as shown in Figure 5.

For illustration purposes, the directional energy distributions of sample shoeprint image blocks are shown in Figure 6. The selected blocks have similar patterns. This similarity is efficiently captured by the DFB energy distribution. The selected image blocks have dominant energies in the 1, 6 and 8 directions.

3.1 Energy-Dominant Block Selection

Based on the DFB energy distribution, the proposed algorithm first finds the energy-dominant blocks in the image (32 or 16 blocks) in an input shoeprint image. To determine the dominant blocks, the proposed algorithm applies a block-based DFB decomposition. The block size is either 32×32 or 16×16 . In the first case, the block overlap includes 16 pixels, while in the second the overlap size is 8 pixels. Then, the DFB energies in each block are computed. According to their energy contribution, the most dominant image blocks are selected. In this paper, either 32 or 16 DFB-dominant image blocks are selected. For each shoeprint block, the DFB energy is computed as follows:

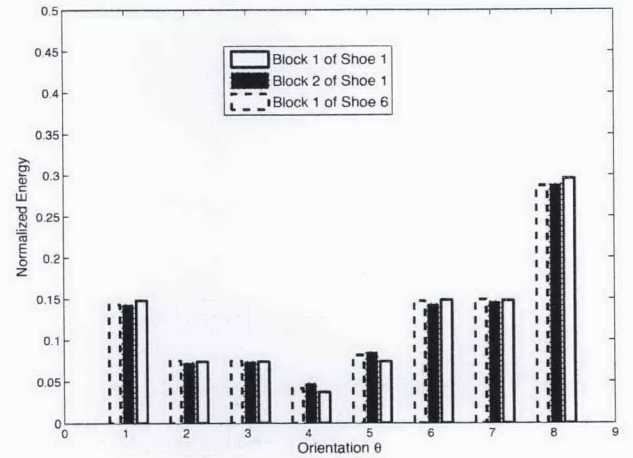


Figure 6: Distribution of directional energies of two sample shoeprint images (Nos. 1 and 6).

$$E_{BLK}^{tot} = \frac{1}{8} \sqrt{\sum_{\theta=0}^7 E_{BLK}^\theta} \quad (4)$$

where E_{BLK}^{tot} is the total DFB energy of the shoeprint block BLK . Based on the contribution of E_{BLK}^{tot} , the first 32 or 16 blocks are retained to contribute to the creation of the feature vector *ShoeHash*.

3.2 Feature Vector Creation

Once the energy-dominant image blocks (32 or 16) are selected, each of these blocks is transformed using the DFB representation presented in Section 2.1. Therefore, for each subband, eight directional subbands are generated. To generate the *ShoeHash* for each DFB block, dominant directional energy components are extracted. However, a threshold is required to differentiate between the block orientations with dominant DFB energy and those with low DFB energy. The generation of the feature vector involves normalized energy values to circumvent the threshold inaccuracies. These inaccuracies are mainly due to spatial intensity variations across the shoeprint. Let E_{BLK}^θ denote the energy content of the DFB subband with direction θ . Furthermore, let \hat{E}_{BLK}^θ correspond to the normalized energy content of E_{BLK}^θ . The feature value, F_{BLK}^θ , is defined below:

$$F_{BLK}^\theta = \begin{cases} \lfloor F_{max} \times \hat{E}_{BLK}^\theta \rfloor & \text{if } \hat{E}_{BLK}^\theta \geq Thresh_{energy} \\ 0, & \text{otherwise} \end{cases} \quad (5)$$

The normalized energy, \hat{E}_{BLK}^θ , is given by:

$$\hat{E}_{BLK}^{\theta} = \frac{E_{BLK}^{\theta}}{\sum_{\theta=0}^7 E_{BLK}^{\theta}} \quad (6)$$

$[x]$ is the nearest integer to x . Instead of using the block energy, E_{BLK}^{θ} , defined in (3), the mean-normalized block energy is used in this paper:

$$E_{BLK}^{\theta} = \sum_{x,y \in BLK} \left| f_{BLK}^{\theta}(x,y) - \bar{f}_{BLK}^{\theta}(x,y) \right|, \quad \theta = 0, 1, 2, \dots, 7 \quad (7)$$

$\bar{f}_{BLK}^{\theta}(x,y)$ is the mean of the element coefficients in the directional block θ . $Thresh_{energy}$ is a threshold value between 0 and 1, and is a positive integer normalization constant. According to (5), the directional energy values with dominant intensity are normalized and quantized to an integer between $(F_{max} \times Thresh_{energy})$ and F_{max} . The least-dominant energy components are considered as noise (set to 0), and thus, discarded. During the computer simulation, F_{max} is set to 255 and $Thresh_{energy}$ is set to 0.12. The latter threshold implies that directional components with energy ratio of less than 12% in each block are discarded. It is worth noting that these threshold values are selected empirically. In summary, the procedure for feature generation is given below:

1. Apply block-based DFB decomposition of the shoeprint image. The output is a set consisting of 32×8 DFB subbands.
2. Extract the most important shoeprint blocks (32 or 16 blocks). The DFB energy calculations are based on (6)-(7)
3. Finally, calculate the feature values from each energy-dominant elements using (5).

Figure 7 shows the generated feature vectors (*ShoeHash*) for two different samples of the same shoeprint and a different shoeprint. For the samples of the same shoeprint, the feature vectors appear similar, yet the feature vectors are quite different for different shoeprint images.

Finally, the shoeprint matching is performed based on finding the normalized Euclidean distance between the input feature vectors and the template feature vector enrolled in the database. Let v_m denote the m^{th} -element in the feature vector of the input shoeprint image and let t_m denote the m^{th} -element in the feature vector of the template shoeprint. The normalized Euclidean distance between the input and template feature vectors, d_{Feat} , is defined below:

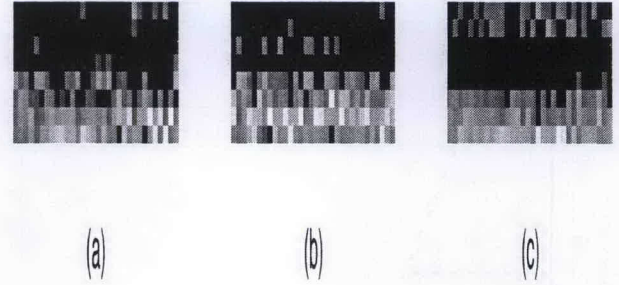


Figure 7: Examples of feature vectors. (a) Original shoe No. 1. (b) Rotated version of shoe No. 1. (c) Original shoe No. 2.

$$d_{Feat} = \begin{cases} (v_m - t_m)^2, & \text{if } v_m \neq 0 \text{ and } t_m \neq 0 \\ 0, & \text{otherwise} \end{cases} \quad (8)$$

4 Experimental Results

For the experiments, we have used two different shoeprint databases provided by the UK Forensic Office and Foster&Freeman Inc., UK. The first database, denoted by *Database 1* consists of 522 shoeprint images, while the second, denote by *Database 2*, consists of 512 images. In both cases, images were scanned using a standard flat bed scanner² with lighting carriage located under the scanned document. The source document consisted of full size shoeprint image at 200 dpi (dots per inch) resolution. All the scanned images were "cleaned up" where grayscale thresholding, image rotation, label removal have been applied. The acquired images were 256 gray scale images and 512×256 in size. All the experiments were conducted on 2 GHz Intel Pentium IV PC using MATLAB environment. Furthermore, for the statistical analysis of the algorithm performance, 9 different samples were generated for each scanned shoeprint image. Shoeprint samples include background addition, image rotation, scaling, contrast adjustment. The background images were selected to represent shoeprint marks collected from SoC locations. It should be noted that the collected databases consist of shoeprints emanating from the most shoe suppliers such as Nike, Adidas, Puma, Reebok, etc. To assess the verification accuracy of the proposed shoeprint matching algorithm, each shoeprint image in each database is matched with all the other shoeprint images in the same database. The genuine and imposter distributions were obtained for the proposed method. Then, based on the characteristics of the latter distributions, the verification performance was assessed. The genuine and imposter distributions provide useful insights about these outcomes. The distribution of the distances between all possible intra-class image pairs in the database are indicated by the former indicates, while the latter represents the distribution

²UMAX Powerlook 2100XL.

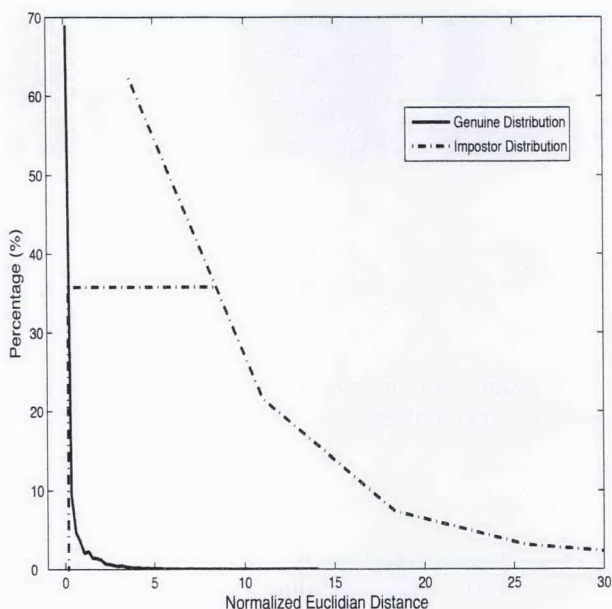


Figure 8: Genuine and impostor distributions for the proposed method using *Database 1* based on 32 DFB blocks.

of the distances between all possible inter-class image pairs in the database. The genuine and impostor distributions of the proposed method is shown in Figure 8 for the case of *Database 1*.

On the other hand, the system errors, characterized by genuine rejection and impostor acceptance outcomes, can be specified by false accept rate (FAR) and false reject rate (FRR). A good system design should minimize the FRR for a given FAR. In fact, there is always a tradeoff between the two system errors dictated by the decision boundary. Acceptance decision is based on a user-defined (or application-dependent) threshold. For a high threshold, the FRR rate is lower but the FAR rate is higher. The receiver operating curve (ROC) can be used to evaluate the performance of a verification system. The ROC produces a graphical representation of the correct acceptance rate (CAR) as a function of the FAR variable. Figure 9 shows the ROC performance using *Database 1*. It is clear from Figures 8-9 that the proposed system has an excellent verification accuracy.

5 Conclusions

In this paper, we have presented a novel multiresolution-based shoeprint feature extraction and matching algorithm. First, the proposed algorithm applies a block-based DFB decomposition of the shoeprint image. Energy-dominant blocks (32 or 16) are selected for the generation of the feature vector of the input shoeprint image. To mitigate the effect of spatial intensity variations, the shoeprint features, *ShoeHash*, are extracted

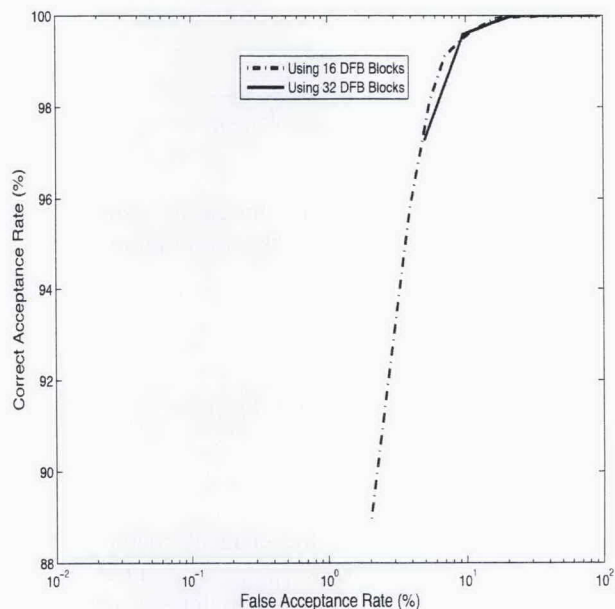


Figure 9: ROC curve for the proposed system using *Database 1* based on 32×32 DFB blocks.

based on the ratios of the directional energy values in each of the extracted blocks. Experimental results using two different shoeprint databases, consisting of more than 1000 images, demonstrate that the proposed shoeprint matching has an excellent verification accuracy.

6 Acknowledgments

This work is supported by ESPRC Grant No. EP/C008057/1. The authors would like to thank Foster&Freeman Ltd. and the UK Forensic Science Services for providing the shoeprint images.

References

- [1] Z. Geradts and J. Keijzer, "The image-database REBEZO for shoe marks with developments on automatic classification of shoe outsole designs," *Forensic Science Int'l*, vol. 82, no. 1, pp. 21-31, 1996.
- [2] "Foster&Freeman Limited," 2006. <http://www.fosterfreeman.co.uk>
- [3] W. J. Bodziak, *Footwear Impression Evidence Detection, Recovery and Examination*. CRC Press, Second Edition, 2000.
- [4] "Daubert Rulings: Footwear Impression Evidence," Apr. 2002. United States District Court - Northern District of Indiana - Fort Wayne Division, USA.

- [5] A. Girod, "Computer classification of the shoeprint of burglar soles," *Forensic Science Int'l*, vol. 82, no. X, pp. 59–65, Sep. 1996.
- [6] R. H. Bamberger and M. J. T. Smith, "A filter bank for the directional decomposition of images," *IEEE Trans. Signal Processing*, vol. 40, no. 4, pp. 882–893, Apr. 1992.
- [7] P. D. Chazal, J. Flynn and R. B. Reilly, "Automated processing of shoeprint images based on the Fourier transform for use in forensic science," *IEEE Trans. Pattern Analysis and Machine Analysis*, vol. 27, no. 3, pp. 341–350, Mar. 2005.
- [8] M. N. Do and M. Vetterli, "The contourlet transform: An efficient directional multiresolution image representation," *IEEE Trans. Image Processing*, vol. 14, no. 12, pp. 2091–2106, Dec. 2005.